

1 Tests on Thin Reinforced Concrete Walls 2 Subjected to In-plane and Out-of-plane Cyclic 3 Loading

4 João Almeida,^{a)} Ovidiu Prodan,^{a)} Angelica Rosso,^{a)} and Katrin Beyer,^{a)}

5 M.EERI

6 The present data paper describes an experimental campaign on five thin T-
7 shaped reinforced concrete walls, including: details on the test units, materials, test
8 setup, loading protocol, instrumentation, main features of each unit's response,
9 organization of the provided test data, and examples of derived data. The tests
10 aimed at assessing the influence of wall thickness on member stability, the role of
11 lap splices on damage distribution and displacement ductility, and the effects of the
12 simultaneous application of out-of-plane loading on the member response. A set of
13 five companion test reports, one for each of the tested units, supplement the present
14 manuscript.

15 INTRODUCTION

16 Recent earthquakes in Chile (2010) and New Zealand (2011) damaged a significant number
17 of buildings with reinforced concrete (RC) walls. Failure modes that were observed after these
18 events included out-of-plane failure of thin walls and failure of walls with lap splices (Kam,
19 Pampanin, and Elwood 2011; Wallace et al. 2012; Elwood 2013; Sritharan et al. 2014). To
20 investigate these failure modes and to analyse the effect of bi-directional loading on wall
21 behaviour, an experimental program consisting of five specimens, tested at a scale that varied
22 between 2/3 and 1/1 (full scale), was carried out at the *Earthquake Engineering and Structural*
23 *Dynamics Laboratory (EESD Lab), École Polytechnique Fédérale de Lausanne (EPFL),*

^{a)} Earthquake Engineering and Structural Dynamics Laboratory (EESD), School of Architecture, Civil and Environmental Engineering (ENAC), École Polytechnique Fédérale de Lausanne (EPFL), 1015 Lausanne, Switzerland

24 Switzerland, with the objective to complement existing data with regard to the aforementioned
25 failure modes.

26 The walls had all the same cross-section (rectangular section with a small flange at one
27 end) but different wall thicknesses and reinforcement layouts. The tests were quasi-static cyclic
28 tests. Only the ground storey of the idealized walls was constructed and the axial force, shear
29 forces and bending moments resulting from the upper storeys were simulated by three (in the
30 uni-directional tests) or five (in the bi-directional tests) servo-controlled actuators. The first
31 three walls (TW1 to TW3) were tested under in-plane loads, while the last two test units (TW4
32 and TW5) were subjected to a combination of in-plane and out-of-plane loads.

33 Wall TW1, which was geometrically identical to wall TW4, was tested in collaboration
34 with the *School of Engineering of Antioquia* and the *University of Medellin*, Colombia.
35 Reproducing a common current Colombian design trend for mid and high rise low-cost
36 residential buildings, walls TW1 and TW4 have only a single layer of reinforcement.
37 Additionally, since those walls have the smallest wall thickness and the largest shear span ratio,
38 they are more prone to instability phenomena. A literature review (Rosso, Almeida, and Beyer
39 2015) on existing wall tests showing global out-of-plane instability of the member revealed
40 that only seven tests from four different campaigns can be found (Oesterle et al. 1976; Goodsir
41 1985; Thomsen and Wallace 1995; Johnson 2010). All of these seven walls were subjected to
42 uni-directional loading and their out-of-plane displacements along the wall height were either
43 observed visually or measured at up to three different heights. The walls TW1 and TW4 of the
44 present test campaign are unique as they provide, for the first time, data on the entire 3D
45 displacement field of walls that develop large out-of-plane displacements. It is expected that
46 these three-dimensional displacement fields of wall faces yield new insights into the
47 development of the out-of-plane deformations, in particular with regard to: evolution of out-
48 of-plane displacements along the height with imposed top in-plane displacements, portion of
49 wall height and length that is involved in the out-of-plane instability, influence of both local
50 and global tensile strains on the buckling behaviour, and role of bi-directional loading on out-
51 of-plane instability (Rosso, Almeida, and Beyer 2016).

52 The geometrical and mechanical properties, as well as reinforcement detailing of test units
53 TW2, TW3 and TW5 is meant to represent Swiss construction practice during the 50s-70s. It
54 was characterized by wall thicknesses between 15 and 20 cm, longitudinal/transversal
55 reinforcement ratios roughly between 0.3 and 0.8%, and transversal stirrups placed on the

56 inside of longitudinal rebars. It is noted that this latter uncommon constructional detail provides
57 an unclear level of confinement to the concrete (which is dependent on the connection between
58 the longitudinal and transversal reinforcement) and restraint against bar buckling. Wall lengths
59 were typically very large, between 4 m and 9 m, while the concrete cover was quite thin, as
60 low as 10 mm. In terms of lap splices, construction practice was to execute lap splices with a
61 considerably low overlapping length of roughly around 30-35 times the diameter of the
62 longitudinal rebar (the current code prescribes an overlapping length of 60 times the diameter).
63 Walls TW2 and TW3 were tested to assess the influence of lap splices in the plastic hinge
64 region. The effect of lap splices in the plastic zone at the wall base has been investigated by
65 six research groups (Paterson and Mitchell 2003; Elnady 2008; Bimschas 2010; Birely 2012;
66 Layssi and Mitchell 2012; Hannewald, Bimschas, and Dazio 2013; Villalobos 2014). Sixteen
67 tests on walls with lap splices could be found in the literature, nine of which can be compared
68 with a reference test without lap splices that has been conducted as well. The newly added pair
69 (TW2, TW3) is unique with regard to its large ratio between lap splice length and shear span,
70 which allows to investigate the effect of the moment gradient on the lap splice performance.

71 Finally, the effect of bi-directional loading on non-rectangular walls has been investigated
72 in a number of experimental studies (e.g. Reynouard and Fardis 1993; Beyer, Dazio, and
73 Priestley 2008; Brueggen 2009; Constantin and Beyer 2015). For rectangular or T-shaped walls
74 such data is, however, not available. In order to address this research gap, walls TW4 and
75 TW5—geometrically identical to walls TW1 and TW2 respectively—have been tested under
76 bi-directional loading.

77 ORGANIZATION OF THE PAPER

78 This paper starts by presenting the geometry and the mechanical characterization of the test
79 units, which is followed by the description of the test setup, the applied quasi-static cyclic
80 loading protocol (both for uni- and bi-directional tests), and the instrumentation used. A
81 summary of each of the test units' response is then presented, as well as the results for the in-
82 plane global force-displacement response. A specific section is dedicated to explain the
83 organization of the data (raw, processed and derived) for the five tests, which are shared online
84 (Almeida, Prodan, Rosso, et al. 2016). Finally, a few examples of plots obtained from derived
85 experimental data are given to illustrate how the data can be used to study local and global wall
86 response parameters.

87

DESCRIPTION OF TEST UNITS AND MATERIALS

88

GEOMETRICAL CHARACTERIZATION

89

The test units were five T-shaped thin walls (the acronym ‘TW’ stands for ‘thin wall’) with a small flange, included to study the effect of a perpendicular wall on member stability and damage distribution. A summary of the main geometrical features, applied loading, and reinforcement details are listed in Table 1. The test units were designed in order to best represent the construction practices described in the Introduction.

94

Walls TW1 and TW4—whose cross-section is depicted in Figure 1(a)—were 2000 mm tall, 80 mm thick and 2700 mm long, with a lateral flange 80 mm thick and 440 mm long (see Figure 1(a)). The longitudinal reinforcement layout consisted of a single layer with 11 bars of diameter $d_w = 6$ mm (resulting in a geometric reinforcement ratio of $\rho_w = 0.15\%$ in the web), three additional bars of diameter $d_b = 16$ mm at the extremities (corresponding to a geometric reinforcement ratio of $\rho_b = 2.63\%$ in the boundary elements), and four bars of diameter $d_w = 6$ mm along the flange. The D6 longitudinal bars of TW1 and TW4 had 350 mm ($\sim 58d_w$) long straight lap-splices at the bottom of the wall; the D16 bars were continuous. The transverse reinforcement ratio consisted of $d_t = 6$ mm bars at a spacing of $s_t = 200$ mm, yielding a geometric reinforcement ratio of $\rho_t = 0.18\%$. The shear span of these walls was fixed at 10 m, which corresponds to a shear span ratio of 3.70.

105

Walls TW2, TW3 and TW5—whose cross-section is depicted in Figure 1(b)—were 2000 mm tall, 120 mm thick and 2700 mm long, with a lateral flange 120 mm thick and 440 mm long (see Figure 1b)). The longitudinal reinforcement layout consisted of a double layer with a total of 58 bars of diameter $d_w = 6$ mm (resulting in a total longitudinal geometric reinforcement ratio of $\rho = 0.57\%$). Test unit TW3 had 216 mm ($36d_w$) straight lap-splices at the bottom of the wall. The transverse reinforcement ratio consisted of $d_t = 6$ mm bars at a spacing of $s_t = 130$ mm (resulting in a geometric reinforcement ratio of $\rho_t = 0.36\%$). In the boundary elements 15 U-shaped rebars of diameter $d_h = 6$ mm at a spacing of $s_h = 130$ mm were placed. The concrete cover was 15 mm. The shear span of TW2 and TW3 was fixed at 3.15 m, which corresponds to a shear span ratio of 1.17. For TW5 the shear span was set to 7.35 m with the objective of rendering it more susceptible to out-of-plane instability.

115

116 The foundation of all the test units was 3600 mm long, 700 mm wide and 400 mm high,
 117 and it was designed as a stiff bearing for the walls. The foundation was fixed to the strong floor
 118 with six prestressed bars.

119 MECHANICAL CHARACTERIZATION

120 Concrete compression tests and double punch tests were carried out on cylinder specimens
 121 to determine the modulus of elasticity, compression strength, and tensile concrete strength for
 122 every wall. The results, corresponding to test averages, are summarized in Table 2.

123 The 6 mm diameter reinforcing steel rebars employed in all test units came from the same
 124 production batch, while the 16 mm rebars used in TW1 and TW4 came from different
 125 production batches. In order to describe their mechanical behaviour, the rebars were subjected
 126 to uniaxial tension tests. The corresponding results are summarized in Table 3.

127 **Table 1.** General geometrical features, applied loading, and reinforcement content of test units.

Test unit	TW1	TW2	TW3	TW4	TW5
Clear unsupported height	2 m	2 m	2 m	2 m	2 m
Length	2.7 m	2.7 m	2.7 m	2.7 m	2.7 m
Thickness	80 mm	120 mm	120 mm	80 mm	120 mm
Shear span	10 m	3.15 m	3.15 m	10 m	7.35 m
Applied shear span ratio	3.70	1.17	1.17	3.70	2.72
Axial load ratio ^a	0.043	0.032	0.034	0.033	0.048
Longitudinal reinforcement	15 × D6 + 6 × D16	66 × D6	66 × D6	15 × D6 + 6 × D16	66 × D6
Total longitudinal reinforcement ratio	0.67%	0.57%	0.57%	0.67%	0.57%
Web longitudinal reinforcement ratio	0.15%	0.50%	0.50%	0.15%	0.50%
Boundary element longitudinal reinforcement ratio ^b	2.63%	0.50%	0.50%	2.63%	0.50%
Lap splice length	350 mm ^c	-	216 mm ^d	350 mm ^c	-
Transverse reinforcement	D6 @ 200 mm	D6 @ 130 mm	D6 @ 130 mm	D6 @ 200 mm	D6 @ 130 mm
Transverse reinforcement ratio	0.18%	0.36%	0.36%	0.18%	0.36%

^aComputed with concrete strength $f_{c,cyl}$ from Table 2. ^bThe boundary element is defined as the 300 mm long region from the web edge where the larger diameter bars are placed. ^cOnly the D6 bars were spliced; the D16 bars were continuous. ^dAll the longitudinal bars were spliced.

128 **Table 2.** Results of concrete compression tests and double-punch tests.

Test unit	TW1	TW2	TW3	TW4	TW5
$f_{c,cyl}$ (MPa)	28.8	50.7	48.3	31.2	33.6
f_t (MPa)	2.2	2.1	2.0	1.5	1.7
E_c (MPa)	25300	31800	30200	29200	31700

Legend: $f_{c,cyl}$: compression concrete cylinder strength, determined from 3/4 tests per test unit. f_t : tensile concrete strength, determined from four double-punch tests per test unit according to equation: $f_t = F / (\pi(1.2rh - a^2))$, where F is the punching force, h and r are the height and the radius of the cylinder respectively, and a is the steel punch radius. E_c : modulus of elasticity determined from the compression tests.

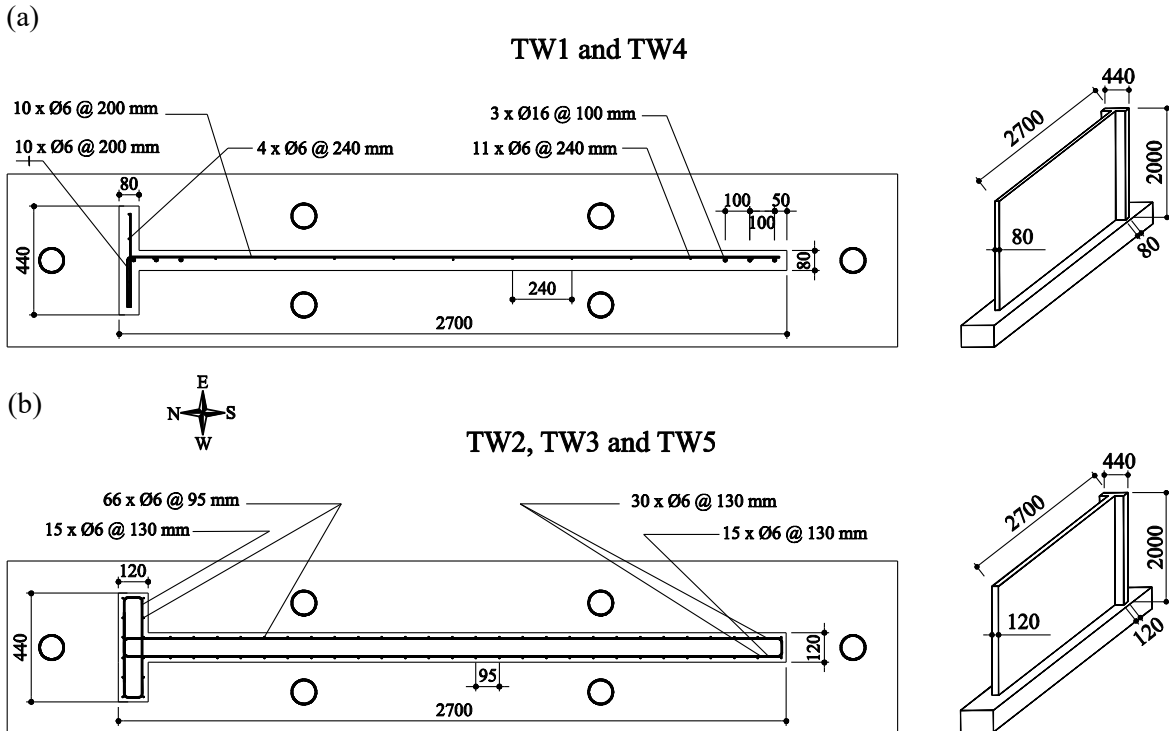
129 **Table 3.** Results of rebar tensile tests.

Diameter of the bars	6	16	
Test units	TW1, TW2, TW3, TW4,	TW1	TW4
$f_{s,y}$ (MPa)	460	565	515
$f_{s,h}$ (MPa)	- ^a	565	515
$f_{s,u}$ (MPa)	625	650	618
$\epsilon_{s,y}$ (%)	2.5	2.7	3.2
$\epsilon_{s,h}$ (%)	- ^a	27	29
$\epsilon_{s,u}$ (%)	99	141	127
E_s (MPa)	184000	208150	- ^b

Legend: $f_{s,y}$: yield strength. $f_{s,h}$: strength at onset of hardening. $f_{s,u}$: ultimate tensile strength. $\epsilon_{s,y}$: yield strain. $\epsilon_{s,h}$: strain at onset of hardening. $\epsilon_{s,u}$: ultimate tensile strain. E_s : modulus of elasticity.

^aThis steel showed no yield plateau. ^bThe value is not provided because of measurement system problems.

130



131 **Figure 1.** Cross-sectional layout and dimensions of the test units (South-East view, top beam not
132 shown) for walls: (a) TW1, TW4; (b) TW2, TW3, TW5. All dimensions are in mm.

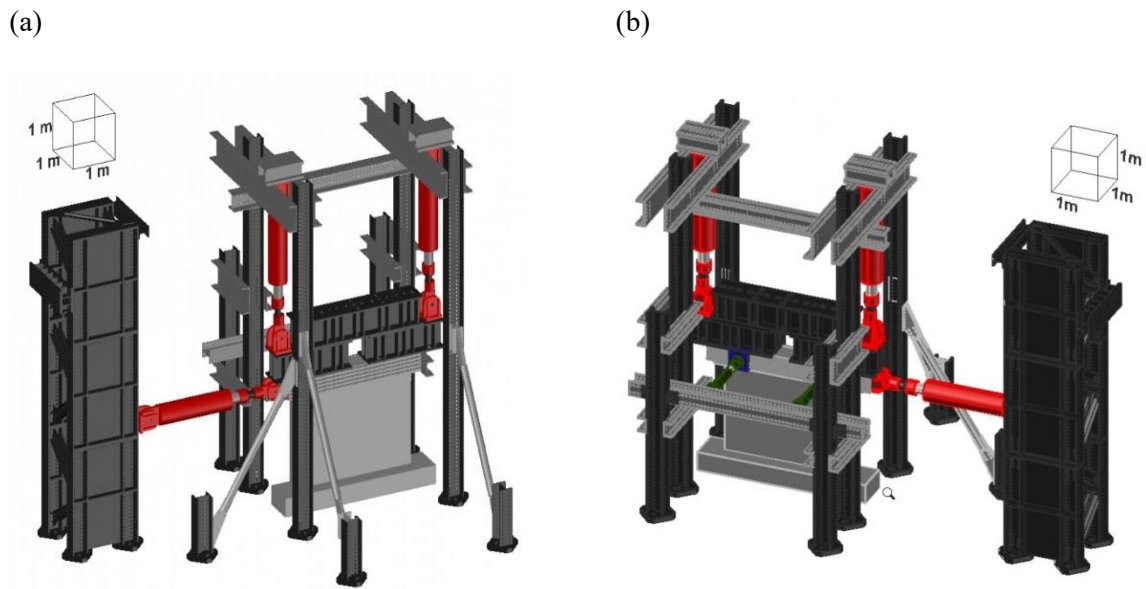
EXPERIMENTAL SETUP AND LOADING PROCEDURE

133

TEST SETUP

134

135 The test setup used for walls TW1, TW2 and TW3 (i.e., subjected to unidirectional loading)
136 is depicted in Figure 2(a), while the modifications put in place for the test of walls TW4 and
137 TW5 are shown in Figure 2(b). The test setup consists of a steel frame, designed to prevent
138 tilting of the wall and to provide a support for the actuators, and a reaction wall. All the steel
139 columns are clamped to the floor with tie rods. Three steel beams are placed over the top RC
140 beam of the test unit to guarantee a distributed application of the loads from the vertical
141 actuators. Such steel loading beams have much larger stiffness and strength than that of the RC
142 wall. Three actuators are employed for the testing of walls TW1, TW2 and TW3: two vertical
143 ones apply the axial load and bending moment corresponding to a chosen shear span ratio
144 through the actuators' lever arm (i.e., the ratio of the moment applied by the vertical actuators
145 to the horizontal force is constant within the test), while the third horizontal actuator applies
146 the cyclic displacement history to the top RC beam of the specimen. The actuators (*Walter+Bai*
147 AG servo-hydraulic actuators with force capacity of ± 1000 kN and total stroke of 1000 mm)
148 are controlled in a fully coupled mode such that the axial force and the height of zero moment
149 remained constant throughout the tests. The horizontal actuator is the master while the vertical
150 actuators are slaved to the previous one. Each actuator is equipped with a load cell and a
151 displacement transducer, used to control the deformation rate. Since the hinges of the actuators
152 have some backlash, external linear variable displacement transducers (LVDTs) are used to
153 measure and control the imposed top displacement of each test unit. In the following, the main
154 sides of the specimen will be identified in accordance to the cardinal points of the *EPFL*
155 Laboratory, see Figure 1: North will be referred as the 'flange side' of the wall, while the South
156 extremity will be referred to as 'web edge'. On the East side an optical measurement system is
157 installed, while on the West side digital image correlation measurement systems are used.
158 During the test of walls TW1, TW2 and TW3, the lateral (East-West) stability of the specimen
159 was guaranteed at the storey level through a bracing system consisting of four steel tubes
160 connected to the top RC beam that allowed for free lateral displacements in the in-plane (North-
161 South) loading direction while restricting such movements in the out-of-plane (East-West)
162 direction. The force in these tubes was derived from measurements by strain gages. On the
163 other hand, the possible development of lateral instability modes over the storey height,
164 triggered by in-plane loading, was intentionally not prevented.



165 **Figure 2.** Test setup used for walls: (a) TW1, TW2, TW3 (North-West view); (b) TW4, TW5 (South-
 166 East view).

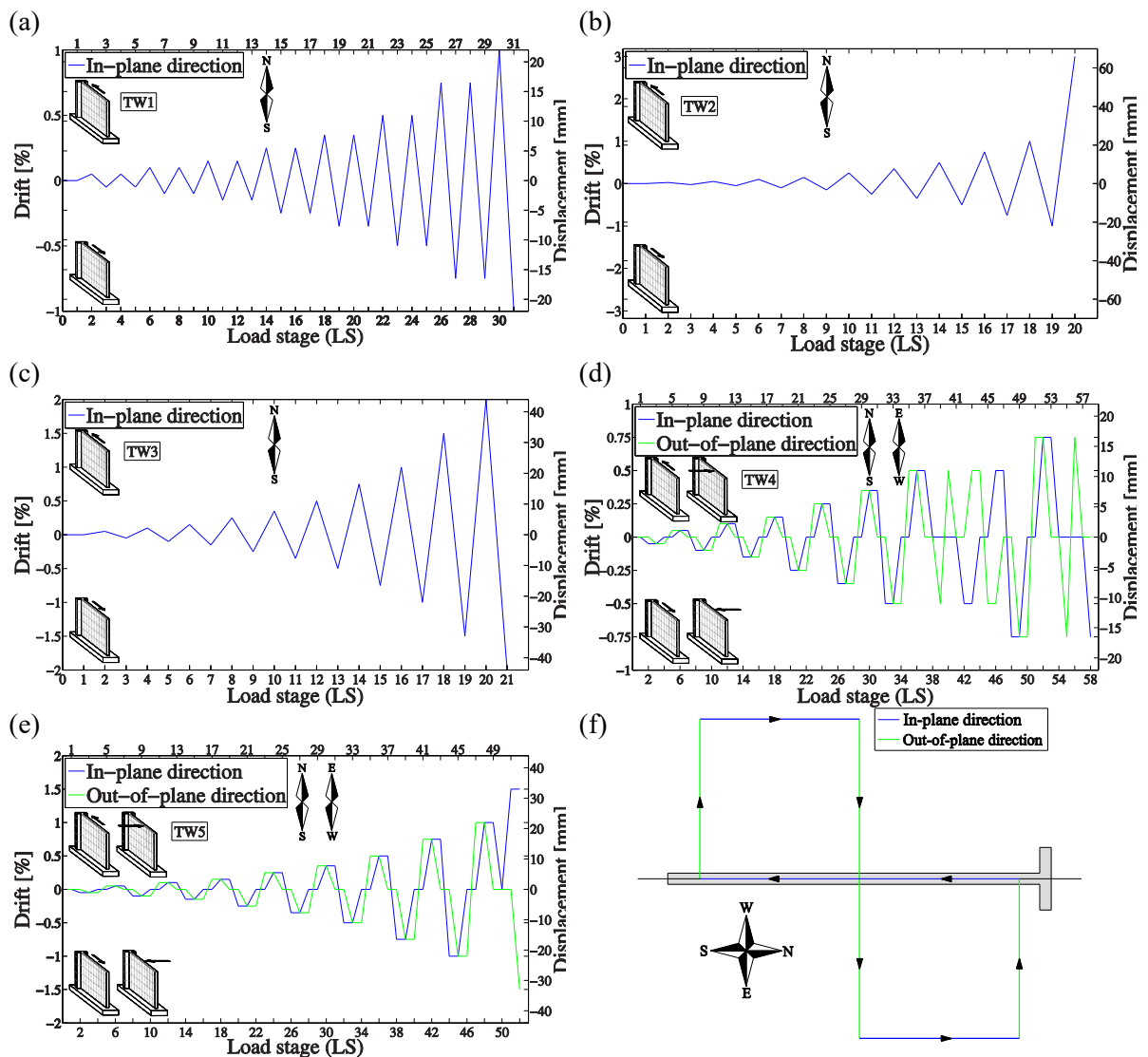
167 For the tests of walls TW4 and TW5, subjected to bi-directional loading, besides the three
 168 actuators previously described, two additional actuators (*Walter+Bai* AG servo-hydraulic
 169 actuators with force capacity of ± 100 kN and total stroke of 200 mm) are placed to apply the
 170 out-of-plane loading. Similarly to the in-plane direction, two external LVDTs are used to
 171 measure the out-of-plane top displacement of the test units.

172 The common approach in RC wall research is to test cantilever walls. Here only a single
 173 storey is tested and the top part of the wall is simulated by the two vertical actuators as
 174 discussed above. The large steel beam at the top of the RC test unit may influence the shear
 175 stiffness and strength of the specimen when compared to a full cantilever wall with multiple
 176 storeys (Brueggen 2009). In real structures, a similar though weaker restraint is provided by
 177 the storey slabs. Since the objective of this test series was not to test shear critical walls, the
 178 approximations introduced by this test setup were judged to be acceptable.

179 **LOADING PROTOCOL**

180 A constant axial load N was applied to the top of the walls such that an axial load ratio of
 181 $v = N/f'_c \cdot A_g \cong 5\%$ was attained at the base of the test units (where f'_c is the design mean
 182 compressive concrete strength and A_g is the gross wall cross-sectional area). Table 1 shows
 183 that, due to the difference between the design mean compressive strength and the results
 184 obtained from cylinder tests (performed after the experiments), the applied axial load ratio at
 185 the base of the wall actually varied between 3.2% and 4.8%.

186 The tests were quasi-static cyclic experiments. The loading protocol consisted of a reversed
 187 cyclic history applied in deformation control. The peak (positive and negative) values of the
 188 imposed (cyclic) drift were named load stages (LS). Figure 3 shows the planned loading
 189 protocols for all the test units, while the reader is referred to each of the individual wall test
 190 reports for comparison with the actually imposed ones (see section ‘Test Data’). Numbering of
 191 the load stages started at LS00 (initial measurements) for the unloaded test unit. LS01
 192 corresponded to the application of the axial load. Each target drift (positive and negative) was
 193 thereafter numbered successively. The displacements in the out-of-plane direction that were
 194 also applied during the tests of TW4 and TW5, in accordance with Figure 3(d) and (e), followed
 195 in general the schema depicted in Figure 3(f); for more detailed information the reader is
 196 referred to the test report of each wall.



197 **Figure 3.** Planned drift history throughout load stages (LS) for walls: (a) TW1; (b) TW2; (c) TW3; (d)
 198 TW4; (e) TW5. (f) Typical loading cycle when bi-directional loading was applied.

INSTRUMENTATION

199

200 All test units were heavily instrumented using conventional instruments and two optical
201 measurement systems. In addition, crack widths were reported, photos were taken, and videos
202 were recorded.

HARD-WIRED MEASUREMENTS

203
204 During the tests up to 54 hard-wired measurements (the actual number depended on the
205 test unit) were recorded. A list of all hard-wired measurements is provided in the test report of
206 each wall.

207 Vertical LVDTs were placed along the edges of each wall, the configuration of which
208 depended on the test unit. Additional LVDTs were placed on the top RC beam at the actuator
209 height to measure the horizontal displacements. The three-dimensional displacement field
210 along the wall surface was measured through optical measurement systems, as discussed in the
211 next two sub-sections. Additionally, for TW4 and TW5 the rotation of the top beam around the
212 North-South (longitudinal) axis was measured using inclinometers. The horizontal forces were
213 measured by the internal load cells of the actuators.

OPTICAL TRIANGULATION MEASUREMENTS

214
215 The three-dimensional displacement field of the surface on the East face of each wall was
216 measured by a grid of infrared light emitting diodes (LEDs). The position of the LEDs was
217 tracked by a camera consisting of three digital optical sensors. To improve the accuracy two
218 cameras were used, each covering about half the wall length. The employed hardware and
219 software was the commercial system NDI Optotrak Certus HD (NDI 2009). The LED grid,
220 whose coordinates were wall-specific, covered the entire wall surface. The LEDs were glued
221 on small metal plates along the grid on the Eastern face of the walls. To measure the
222 displacements of the foundation and of the top RC beam, small L-shaped steel brackets with
223 attached LEDs were glued to these two elements. The LEDs on the top row were hence
224 measuring the displacement of the top beam located 20 mm above, while those on the bottom
225 row measured the displacement of the foundation located 12 mm below.

226 Upon data post-processing, the LED coordinates were transformed to the following spatial
227 reference system: the x-axis refers to the horizontal in-plane direction of the wall (positive
228 direction from the web to the flange), the y-axis to the vertical in-plane direction (positive
229 direction from bottom to top), while the z-axis refers to the out-of-plane direction (positive

230 direction from West to East, see Figure 1). The origin of the coordinate system is in the South
231 bottom corner.

232 The LED data was collected not only during loading (i.e., in-between consecutive load
233 stages), but also during approximately two minutes at each load stage (i.e., for constant values
234 of imposed horizontal displacements).

235 **DIGITAL IMAGE CORRELATION MEASUREMENTS**

236 A speckle pattern for digital image correlation (DIC) measurements was applied on the
237 West face of each wall. As DIC on large surfaces had not been used in the structural
238 engineering laboratory at *EPFL* before, different speckle patterns and camera configurations—
239 sometimes used in parallel—were tested.

240 For TW1 to TW3, which were subjected to in-plane loading only, a two-dimensional DIC
241 system (DIC system 2D 1) was used. The system was composed of two Nikon D800 cameras,
242 each recording an area of approximately 0.7m x 0.7m at the two bottom wall corners. The exact
243 size and position of these areas varied between walls and is indicated in the test report
244 accompanying each test. For TW3, a second 2D system (DIC system 2D 2) was used. The
245 system was composed of one Canon EOS 5D Mark II camera and recorded the entire wall
246 surface (without the flange). The speckle pattern used for the first three specimens was sprayed
247 with pressured air.

248 TW4 and TW5 were subjected to bi-directional loading and therefore 3D rather than 2D
249 DIC systems were used. For each wall two 3D systems were used, each recording the entire
250 West face. The first one was composed of two industrial Manta cameras (DIC system 3D 1)
251 and the second one of two Nikon D800 cameras (DIC system 3D 2). The first system recorded
252 black and white photos while all other cameras recorded colour photos. The black and white
253 photos are smaller size files while simultaneously the sensor's larger dimensions mean that
254 they have a higher resolution. The speckle pattern was applied by means of a stencil with a
255 computer generated pattern. The black colour was applied with a spraying can.

256 **CRACK WIDTHS, PHOTOS AND VIDEOS**

257 The maximum crack width, as well as the widths of several cracks developing in the walls,
258 were measured manually at most load stages using a crack-width comparator and are recorded
259 in the lab books, which are made available. Photos of all faces of each test unit were taken at
260 every load stage, as well as of all relevant signs of local damage (cracks, spalling, splitting or

261 crushing of concrete, rebar buckling and fracture, etc). Moreover, videos of the wall
262 deformation occurring in-between successive load stages were made. These resources proved
263 very useful in the *a posteriori* analysis of the wall behaviour, contributing to a better
264 understanding of the progression of damage and the transfer of forces between distinct
265 deformation modes of the member.

266

TEST OBSERVATIONS

267 The following sub-sections present a summary of each member response and a brief
268 discussion on the mechanisms that led to failure.

269

TW1

270 Figure 4(a) shows the in-plane force-displacement responses of wall TW1, wherein a stable
271 hysteretic behaviour with appreciable dissipation of energy can be observed. Focusing on the
272 last cycle, i.e. while loading towards -1% drift (LS30→LS31), clear signs of cyclic strength
273 degradation can be observed: upon reaching the target drift of the previous cycle (-0.75%), the
274 in-plane force capacity of the wall was approximately 40% smaller. Continuation of loading
275 led to wall failure due to concrete crushing and buckling of rebars. It is noted that the strength
276 degradation appears to have initiated when returning from positive drifts and approaching zero
277 in-plane drift, where the out-of-plane displacement along the wall height was maximum. At
278 that point, it was apparent that the force-displacement curve deviated from the branch
279 corresponding to the previous loadings towards -0.75% drift.

280

281 Cracks following a mainly horizontal pattern started forming from the first loading cycles,
282 indicating a flexural type of behaviour. Although the wall was loaded in-plane, when loading
283 first to -0.75% drift (LS26→LS27), the wall started to show evident out-of-plane
284 displacements along the height towards West, but the latter were recovered completely before
285 reaching the target drift. A similar behaviour with even larger out-of-plane displacements was
286 observed during the second cycle at -0.75% drift (LS28→LS29). During loading at -1% drift,
287 following the large out-of-plane deformations depicted in Figure 4(f) and the progression of
288 concrete crushing, a local buckling of the longitudinal rebars in the bottom region of the web
289 edge took place, see Figure 4(g). The failure mode was thus an in-plane failure triggered by
290 damage induced by out-of-plane deformations (Rosso, Almeida, and Beyer 2016). The splicing
of the D6 longitudinal bars did not seem to have affected the wall performance.

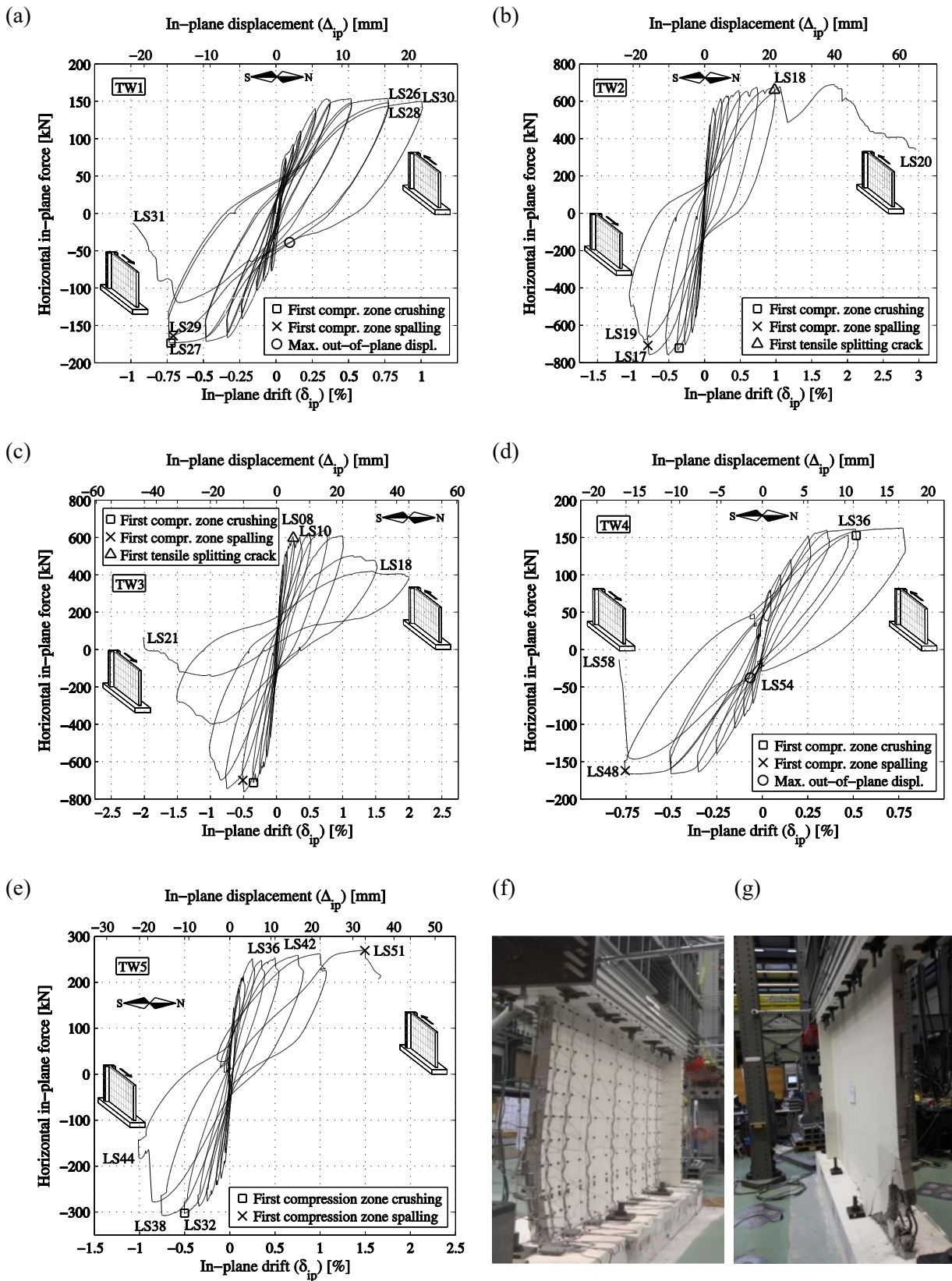
291 **TW2**

292 Figure 4(b) shows the force-displacement response of wall TW2. It shows stable hysteretic
293 loops up to -0.75% drift when loading towards the web side (LS17). During the following cycle
294 in the same direction (LS19), at -1% drift, the wall lost almost half of its horizontal force
295 capacity, indicating the attainment of failure. As expected, when loading towards the flange
296 side (even values of load stages), the member depicted a much more ductile response and only
297 showed signs of degrading force capacity above drifts of 1.75%. Failure in this direction can
298 be considered to have occurred at around 2.2% drift, corresponding to an approximate drop of
299 20% of the member capacity. It should be noted that, in Figure 4(b), there is an abrupt drop in
300 the force-displacement response of the test unit at around 1.2% drift. Such drop does not
301 correspond to any physical phenomenon but rather to the pressing of the ‘emergency stop’
302 button of the oil pressure system feeding the actuators. This was done as it was feared that a
303 possible collapse could be imminent, putting at risk the integrity of diverse laboratory
304 equipment (e.g. LVDTs, which were therefore removed).

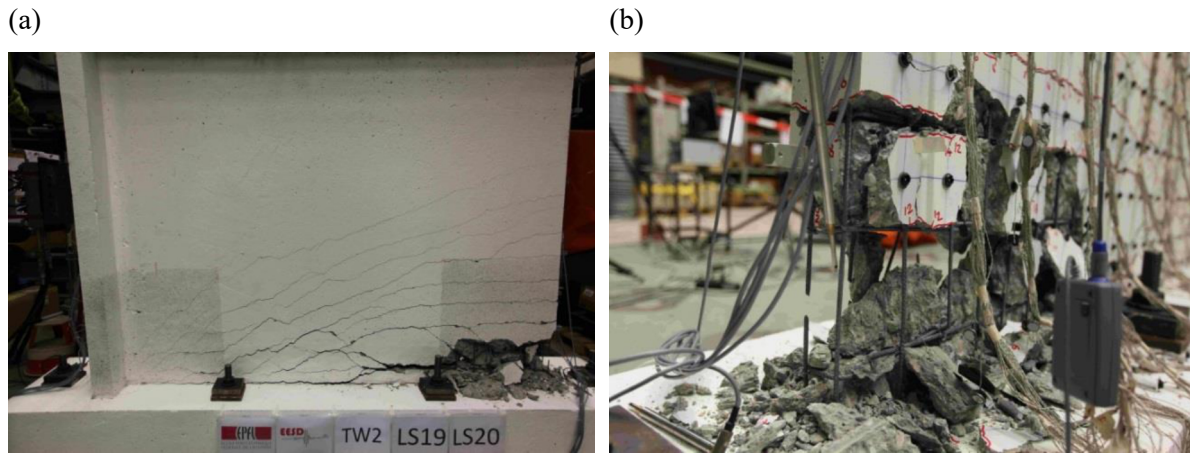
305 The first visible crack was detected at LS06, corresponding to a very small drift of 0.1%.
306 Compression crushing of the concrete cover was signalled by the appearance of the first vertical
307 cracks in the web edge of the test unit (LS13). The horizontality of the wall cracks indicates a
308 predominantly flexural type of member behaviour in an initial phase. At load stage LS17, the
309 concrete spalled off along a height of approximately 10 cm at the web edge base.

310 When continuing loading to LS19, extensive crushing of the concrete at the web edge
311 bottom region took place, which affected the load carrying capacity of the wall and induced
312 the failure of the member in this direction. Hence, it was decided to not reload again the wall
313 in the same direction. During the following load reversal to LS20, the wall showed a stable
314 ductile behaviour up to around 2% drift, at which point concrete cover spalled off.

315 The progressive loss of the wall capacity beyond 2% drift was not related to concrete
316 crushing in the flange but can be attributed to the consecutive fracture of longitudinal rebars at
317 the (opposite) web edge, which was distinctly heard during the test. Figure 5 shows the
318 condition of the test unit at the end of the experiment. It should be noted that very small out-
319 of-plane displacements were observed (less than 1 cm). Further information about the response
320 of TW2 can be found in Almeida et al. (2015).



321 **Figure 4.** In-plane force-displacement response for walls: (a) TW1; (b) TW2; (c) TW3; (d) TW4; (e)
 322 TW5. (f) Deformed shape of wall TW1 when loading to -1% drift. (g) TW1 at the end of the test, after
 323 failure.



324 **Figure 5.** (a) Overview of wall TW2 condition at final load stage LS20. (b) Close-ups at web edge,
 325 depicting rebar fracture.

326 **TW3**

327 The force-displacement response of wall TW3 is shown in Figure 4(c). Comparing the
 328 results of this wall with TW2, it can be observed that the response is quite similar when loading
 329 towards the web edge side (negative values of drift). On the other hand, when loading occurs
 330 towards the flange edge side (positive values of drift), the test unit does not attain quite the
 331 same value of force capacity, and the degradation of strength starts at a lower drift level of
 332 0.75%. The drift level corresponding to an approximate drop of 20% of the member capacity
 333 is 1.15%, which represents roughly 50% of the corresponding drift capacity of TW2. The local
 334 effects caused by the presence of lap splices can explain this comparative decrease of the wall
 335 performance at the global level.

336 The first face-splitting vertical cracks at the web edge of TW3 appeared as early as load
 337 stage LS08 (corresponding to a drift of 0.25%) along the upper half of the lap splices, indicating
 338 the significant transfer of tensile stresses between the rebars and the surrounding concrete in
 339 the lap splice region, and possibly yielding of the rebar. At LS10 (0.35% drift), a very clear
 340 side-splitting crack at the web edge extremity also showed up extending over approximately
 341 the entire height of the lap splice.

342 The crack pattern showed that a concentration of deformation above the lap splice took
 343 place. When the web edge was in tension, a single large crack at about the top end of the lap
 344 splice opened up (22 cm above the foundation, Figure 6(a)). Simultaneously, the cracks above
 345 the lap splice started to reduce their width in comparison with previous load stages. For loading
 346 in the other direction, concrete crushing localized in the large crack above the lap splice, see
 347 Figure 6(b). An inspection of the aforementioned crack at the end of the test shows that the

348 tensile failure involved a combination of rebar fracture and bond-slip (Almeida, Prodan,
349 Tarquini, et al. 2016). As already observed for TW2, very small out-of-plane displacements
350 occurred (less than 1 cm).

351 **TW4**

352 Figure 4(d) shows the in-plane force-displacement response of TW4 (it is recalled that both
353 top in-plane and out-of-plane displacements were applied to this wall, as well as for TW5).
354 During the last cycles, when loading from the flange to the web edge, the wall showed clear
355 signs of cyclic strength degradation. During the last loading cycle (towards -0.75% drift), the
356 in-plane capacity of the wall at -0.70% drift was approximately 90% of the strength at the
357 previous cycle at -0.75% drift (LS48), which was then followed by a sudden drop in resistance.

358 Wall TW4 showed a predominantly flexural behaviour from the first load stages, with the
359 appearance of mainly horizontal cracks. At 0.5% drift (LS36) crushing of the concrete was first
360 observed, occurring at the wall base of the web edge. From LS38 onwards the wall developed
361 an out-of-plane deformed shape towards West (similarly to wall TW1). At -0.75% (LS48) the
362 first concrete spalling took place (Figure 7(a)). During the second cycle at -0.75% drift
363 (LS57→LS58), following progression of concrete crushing and spalling of cover concrete—
364 partially promoted by rebar buckling—a sudden failure took place. After an increase of the
365 overall out-of-plane displacement along the wall height, then completely recovered (Figure
366 7(b)), the failure involved abrupt concrete crushing and buckling of the rebars in the boundary
367 element of the web edge, as depicted in Figure 7(c). An extensive comparison between TW1
368 and TW4—which were geometrically identical—can be found in Rosso, Almeida, and Beyer
369 (2016).

370 **TW5**

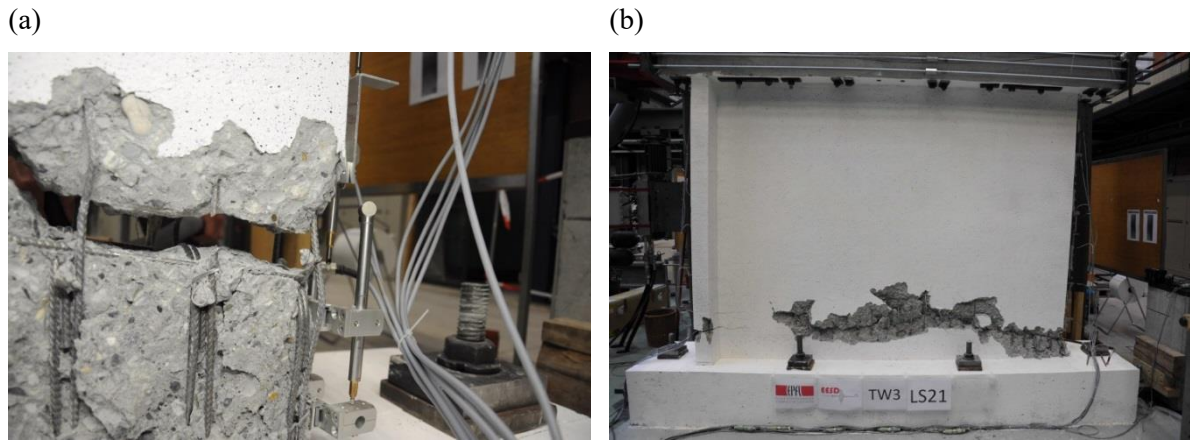
371 Wall TW5 depicted a relatively fat hysteretic in-plane force-displacement response, as
372 shown in Figure 4(e). This can be associated to the clear predominance of flexural
373 deformations, as evidenced by a stable development of well distributed horizontal cracks along
374 the wall height, both from the flange and the web edges. The vertical distribution of these
375 cracks was much larger than those of the identical wall TW2, as observable from the
376 comparison between Figure 8(a) and Figure 5(a), which is directly attributable to the imposed
377 shear span ratio, almost 2.5 times larger in wall TW5 (see Table 1). Only in the later load

378 stages, corresponding to larger in-plane drifts, did rather inclined shear cracks show up to
379 bridge between the tensile and compressive zones.

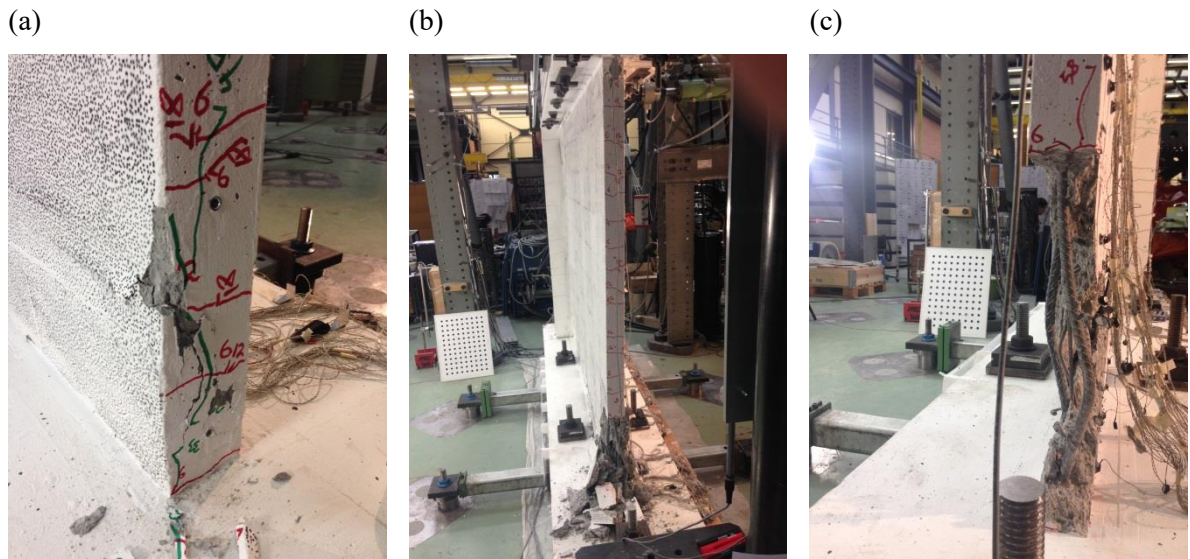
380 The first horizontal cracks from the web edge appeared at LS06—corresponding to an
381 incipient imposed drift of 0.05% (both in- and out-of-plane), and from the flange edge at
382 LS08—corresponding to an also small in-plane drift of -0.1%. The first vertical crushing cracks
383 were observed at absolute in-plane drifts of 0.5% for both directions (i.e., at LS32 for the web
384 edge, and at LS36 for the flange edge, in the latter case while a simultaneous out-of-plane drift
385 of 0.5% was also being applied). At the following drift level of 0.75%, extensive crushing and
386 concrete spalling occurred while loading towards the web edge (LS38), while in the opposite
387 direction only minimal spall-off could be observed at the flange corner under maximum
388 compression from bi-directional loading (LS42). Finally, specimen failure occurred at LS44
389 during in-plane loading towards -1% drift: as illustrated in Figure 8(b), generalized crushing at
390 the web edge took place. However, the sudden drop of around 35% on the lateral load capacity
391 can also be ascribed to the buckling of the two outermost layers of longitudinal reinforcement.

392 When the web edge failed, the flange side was not significantly damaged and therefore the
393 test was continued. After having completed the cycle at 1% drift the wall was unloaded to the
394 zero position and then it was loaded again to the flange direction. After attaining an imposed
395 level of 1.5% in-plane drift (LS51), and while trying to load to -1.5% out-of-plane drift
396 (LS51→LS52), the in-plane force capacity dropped significantly—due to concrete crushing
397 and spalling at the Western side of the flange—and the test was hence stopped.

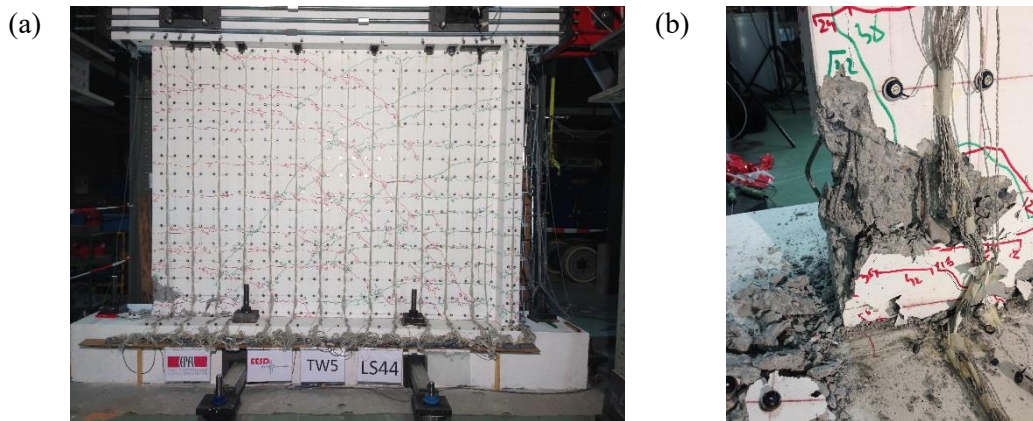
398 Apart from this last cycle, the influence of the imposed out-of-plane displacements does
399 not seem to have significantly affected the member response since the load stages
400 corresponding to the application of out-of-plane displacements only minimally influenced the
401 resisting in-plane lateral load, and further produced only a relatively minor increase of pre-
402 existing cracks, concrete crushing and spalling. However, such effect was visible in the flange,
403 suggesting that the study of the effects of out-of-plane loads on barbelled walls may be worth
404 pursuing.



405 **Figure 6.** (a) Load stage LS18 for wall TW3: crack of 35 mm width at about lap splice level (22 cm
 406 above the foundation), extending along a length of around 100 cm. (b) Final condition of wall TW3.
 407 Crushing from the web edge extends throughout a length of about 220 cm.



408 **Figure 7.** (a) Load stage LS48 for wall TW4: concrete spall-off at the web edge. (b) Final condition of
 409 TW4: the relevant out-of-plane displacements that occurred during the test cannot be observed in the
 410 final collapsed state. (c) Close-up of rebar buckling after failure.



411 **Figure 8.** (a) General condition of wall TW5 at horizontal failure (loading towards the web edge, at
 412 load stage LS44). (b) Detail of the crushing zone, with buckling of longitudinal rebars.

413

TEST DATA

414

ORGANIZATION OF THE DATA

415

416

417

418

419

420

All test data can be downloaded from a publically accessible platform (Almeida, Prodan, Rosso, et al. 2016). The structure of the data folders is summarized in Figure 9. The data is organized by specimen, with specific folders for each test unit “TW(i)”, whilst in a further folder (“Overview”) copies of the most relevant files are provided. This latter folder is thought for readers who want to get a general idea of the walls’ response without downloading the complete data set.

421

OVERVIEW

422

423

424

425

426

The folder “Overview” contains a summary of the five wall tests. Firstly, the test reports for each test unit are provided (“TW(i)_Specimen_description.pdf”). Then, in the sub-folder “Photos”, a collection of the most interesting images of the specimens is grouped. The sub-folder “Postprocessed data” contains the post-processed data from the conventional instruments and LEDs for each wall. For a description of these files see the following section.

427

TW(i) FOLDERS

428

429

430

431

The data is organized first by specimen. In Figure 9 the folders for a generic wall TW(i) are represented; this data structure corresponds to the most general layout, although for each specimen smaller differences may show up since the instrumentation was not exactly the same for all the tests. Three main folders can be downloaded for each test unit:

432

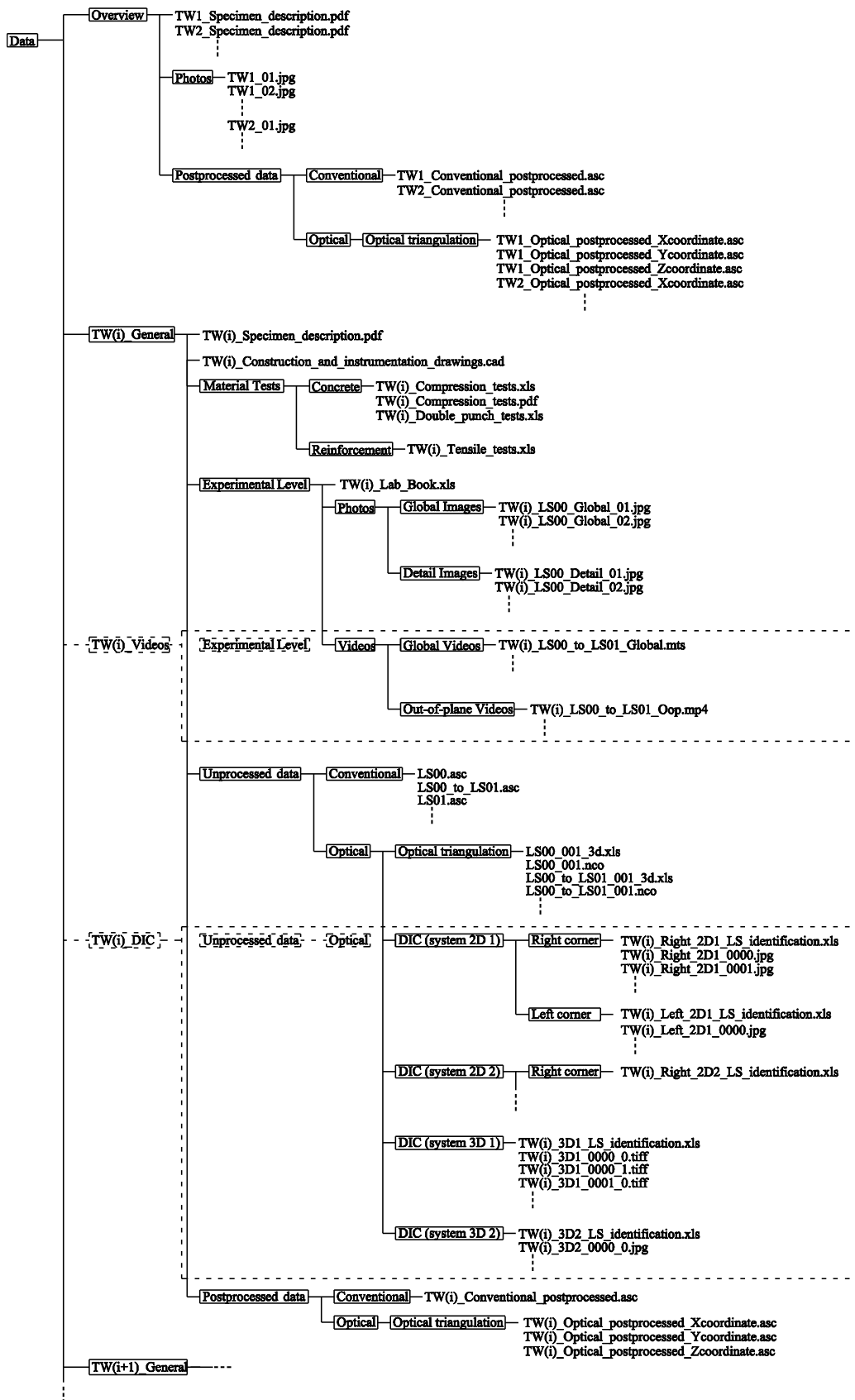
433

434

435

436

1. “TW(i)_General”: it contains a test report summarizing the characteristics and the specific test details of wall TW(i) (called “TW(i)_Specimen_description.pdf”, which follows the structure of the current paper) and a file with the drawings of the geometry, reinforcement, and instrumentation (called “TW(i)_Construction_and_instrumentation_drawings.dwg”). Additionally, the folder is divided into four sub-levels:



437

438 **Figure 9.** Layout of test data organization (boxes with dotted lines enclose folders that can be
439 downloaded separately from “TW(i)_General”).

440 (i) “Material Tests”: two sub-folders contain the results of the material tests
441 performed on the “Concrete” (compression tests and double punch tests) and on the
442 “Reinforcement” (uniaxial tensile tests). Further information on how these tests were
443 carried out can be found in the specific test reports.

444 (ii) “Experimental Level”: a copy of the laboratory notebook, which records
445 observations made during the experimental test, is provided in the form of an Excel
446 spreadsheet (named “TW(i)_Lab_Book.xls”). Two main sub-folders, “Photos” and
447 “Videos”, are part of this sub-level. The latter is downloadable in a separate file, see
448 point 2 below (“TW(i)_Videos”). The former collects the main photos of the test; in
449 particular, the sub-folders “Global Images” and “Detail Images” provide images of the
450 entire wall and of interesting details of the specimen (taken at the load stages)
451 respectively. The images and the videos were named “TW(i)_LS(j)” or
452 “TW(i)_LS(j)_to_LS(j+1)” when recorded at a load stage (j) or in-between two load
453 stages (j) and (j+1) respectively.

454 (iii) “Unprocessed Data”: part of the sub-folders forming this sub-level are
455 downloadable in a separate file, see point 3 below (“TW(i)_DIC”). The current file
456 contains the original recordings from the conventional and optical measurement
457 systems; in the “Conventional” folder the original output files of the system *CATMAN*
458 (HBM 2000), used to record the conventional measurements (LVDTs, load cells, ...),
459 are collected. It is noted that the channel referring to the optical triangulation system
460 reports simply when the optical system was recording. The conventional measurements
461 were always started before and stopped after the optical measurements and this voltage
462 signal was therefore used to synchronize the two systems. In the folder “Optical
463 triangulation” the outputs from the LED measurement system are collected. For each
464 recording sequence the raw data is provided in an Excel file (extension “.xls”) and the
465 sensor settings in NDI-specific file formats (extension “.nco”). In each Excel
466 spreadsheet the actual measurements are organized in columns: the first column stores
467 an index starting from 1, while the following columns give the coordinate
468 measurements of the LEDs (each three columns store the x-, y-, and z-coordinate
469 measurements of one LED respectively). Note that the LED numbers are at this stage
470 still unorganized and the numbering indicated in these files does not correspond to the
471 LED numbering of the processed data. If the LED-coordinates of a LED were not

472 measured (because the LED was not visible or because it fell off during the test), the
473 columns corresponding to such LED do not contain any entries. The origin of the
474 reference system of the raw data is the centre of the master sensor.

475 (iv)“Post-processed Data”: the optical triangulation data was post-processed in
476 order to synchronize the conventional and the optical measurement systems to reduce
477 the amount of data, and to remove any bias or data that is not linked to the actual
478 behaviour of the test unit (e.g. data was removed when a LED fell off). The data is
479 again divided in two folders: “Conventional” and “Optical”. In the file
480 “TW(i)_Conventional_postprocessed.asc”, the columns represent a specific
481 measurement—as described in the test report relative to the specimen,
482 “TW(i)_Specimen_description.pdf”—during the entire test; in the files
483 “TW(i)_Optical_postprocessed_(k)coordinate.asc” the first row indicates the LED
484 numbers—according to the description shown in the aforementioned test report—and
485 the corresponding columns below report the measured displacement along the (k)
486 coordinate—x, y or z—of the LED during the test. Note that, due to distinct events that
487 occurred during the experiments—as described in the previous paragraph—some
488 channels were not post-processed up to the last load stage of the test.

489 2. “TW(i)_Videos”: two different video angles were used; from the West the in-plane
490 response of the entire wall was recorded (see folder “Global Videos”) while from the South the
491 member response was filmed in order to capture possible out-of-plane displacements (see
492 folder “Out-of-plane Videos”). Due to space constraints, just the last load stages or those
493 considered potentially interesting for the readers were included in the database.

494 3. “TW(i)_DIC”: this folder collects the photos taken for the application of DIC post-
495 processing techniques. Photos from each DIC system are organised in different sub-folders
496 (see section ‘Digital Image Correlation Measurements’). In each sub-folder the photos taken
497 during the calibration are the first to be provided, followed by images taken in-between and at
498 the single load stages. In each folder an Excel file (extension “.xls”) is provided in which the
499 numbering of the photos is related to the load stages. Note that for the 2D systems, “Right” and
500 “Left” refer to the corresponding corners, while for the 3D systems “_0” refers to the left
501 camera whilst “_1” stands for the right one. Since the cameras of the digital image correlation
502 systems were not connected to the system measuring the conventional instruments, the
503 synchronization between the data and the photos can only be carried out at the level of the

504 “Unprocessed data” through the corresponding file date settings (all the internal camera clocks
 505 were manually synchronized before each test).

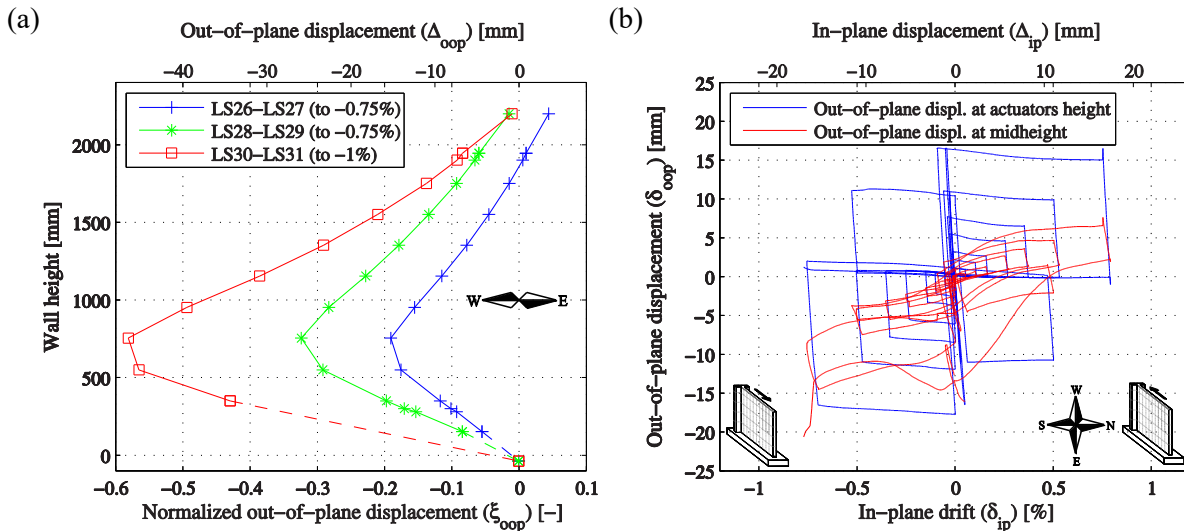
506 **EXAMPLES OF DERIVED DATA**

507 This section includes some examples of plots and figures that can be produced using the
 508 provided experimental data. All plots are created using the post-processed data.

509 **EXAMPLE PLOTS FOR GLOBAL BEHAVIOUR**

510 The test unit TW1 showed a global behaviour influenced by out-of-plane deformations.
 511 The optical measurements taken during the tests allow plotting the evolution of the deformed
 512 shapes of the walls. Figure 10(a) depicts the out-of-plane displacement profile of the web edge
 513 (i.e., the outermost column of LEDs) in-between several load stages: it can be seen that large
 514 values of the out-of-plane displacement were attained.

515 Test unit TW4 was subjected to bi-directional loading. Figure 10(b) shows the out-of-plane
 516 displacement against the in-plane displacement at the height of the horizontal actuators (blue
 517 line). It can be compared with the out-of-plane displacement at midheight of the web edge (red
 518 line), which shows an asymmetric behaviour for the two in-plane loading directions. When
 519 loading towards the web (negative in-plane direction), the out-of-plane displacements at
 520 midheight are considerably larger than when the wall is pushed towards the flange (positive
 521 in-plane direction). This is because the flange is more stable in compression than the web edge.

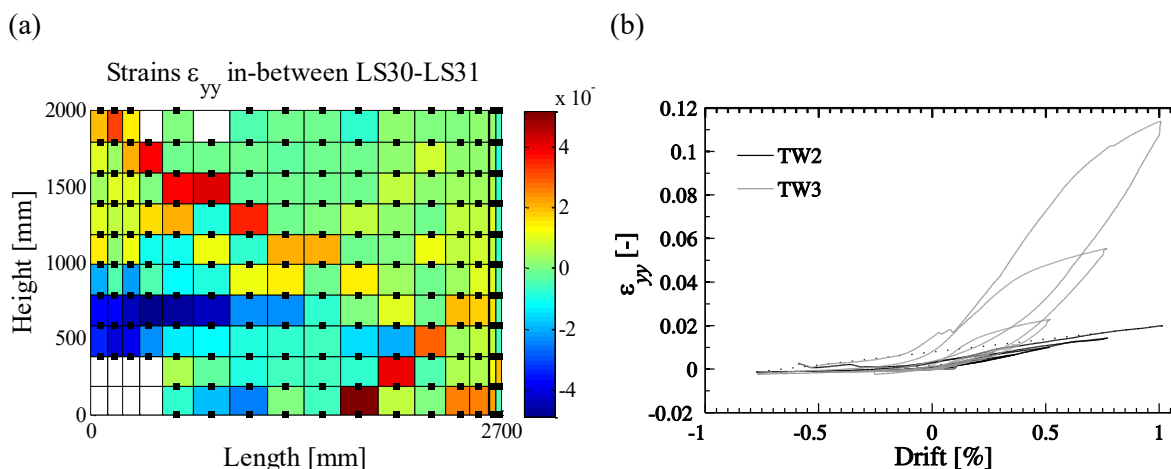


522 **Figure 10.** (a) Web edge out-of-plane displacement profile along the wall height between consecutive
 523 load stages for wall TW1. (b) In-plane displacement *versus* out-of-plane displacement for wall TW4.

524 **EXAMPLE PLOTS FOR LOCAL BEHAVIOUR**

525 The optical measurement data can also be used to compute local deformations, such as
 526 strains and crack widths. Figure 11(a) shows the distribution of the axial vertical strains of
 527 TW1 when the maximum out-of-plane displacement along the wall height was attained (i.e.,
 528 during loading LS30→LS31); the plot points out how the compressive strains concentrate in
 529 the web edge at around 755 mm from the base foundation, providing an idea of the band at the
 530 wall mid-height in which cracks closure causes the reduction of the global out-of-plane wall
 531 deformations.

532 Test unit TW3 differed from TW2 in the inclusion of lap splices at the wall base. As
 533 described in the section ‘Test Observations’, such constructional detail induced a distinct local
 534 and global behaviour of the member. In particular, a large crack formed around the top of the
 535 lap splices. In test unit TW2 the deformations spread over a plastic region near the wall base.
 536 This difference in behaviour is illustrated in Figure 11(b), which shows, for both test units, the
 537 local vertical strains in the web edge region at the crack height; they correspond to the average
 538 of the strains from four consecutive pairs of LEDs (along the wall length) above and below the
 539 top extremity of the lap splices (i.e., between markers no. 2-3, 18-19, 34-35, and 50-51, see
 540 corresponding test reports). It can be seen that, for test unit TW3, strains concentrate at much
 541 lower values of in-plane drifts when compared to TW2, putting into evidence the
 542 abovementioned differences at the local level.



543 **Figure 11.** (a) Distribution of local axial vertical strains throughout the wall when the maximum out-
 544 of-plane displacement was attained for TW1, during loading LS30→LS31 (the two LED rows at around
 545 340 mm above the base were removed for computation and plotting purposes). (b) Averaged local
 546 vertical strains in the web edge region, at a height corresponding to the crack developing at about the
 547 top extremity of the lap splices (the last data entries were manually removed for plotting purposes).

SUMMARY

548

549 The paper presented the data of five quasi-static cyclic tests on thin T-shaped RC walls,
550 which is made publically accessible. The tests are unique with respect to the following aspects.
551 TW1 and TW4 are the first tests on RC walls that developed large out-of-plane displacements
552 along the wall height for which the entire 3D displacement field was measured. The pair TW1-
553 TW4 allows to compare the response of a wall subjected to uni-directional loading (TW1) to
554 that of an identically constructed specimen subjected to bi-directional loading (TW4). TW3 is
555 the wall test with the largest lap splice length to shear span ratio (among those that the authors
556 could find in the literature) and, when compared to other tests on walls with lap splices, shows
557 therefore the influence of the moment gradient on lap splice performance. The corresponding
558 reference test unit with continuous reinforcement that serves as a benchmark was TW2. Wall
559 TW5 is geometrically and mechanically similar to unit TW2, but was loaded under bi-
560 directional loading (with a larger shear span ratio). Test units TW4 and TW5 are one of the
561 first bi-directional wall tests on nearly rectangular walls and allow therefore to make an initial
562 assessment of the impact of bi-directional loading on wall performance.

563 The walls tested correspond to the bottom storey of the idealized building, where inelastic
564 deformations concentrate. The axial force, shear force and bending moment that resulted from
565 the upper storeys were simulated by three (in the uni-directional tests) or five (in the bi-
566 directional tests) coupled servo-controlled actuators. The walls were extensively instrumented
567 using conventional instrumentation and two optical measurement systems (an LED-based
568 triangulation system and digital image correlation systems) providing therefore a wealth of
569 information not only at the global but also at the local level. Such data is important to
570 understand wall behaviour but also to validate numerical models.

571

ACKNOWLEDGMENTS

572 The testing of test unit TW1 was financed through an *EPFL Seed Money* grant of the *EPFL*
573 *Cooperation & Development Center (CODEV)*, which was awarded to the *EESD group* (PI)
574 and the *School of Engineering of Antioquia* and the *University of Medellin*, in Colombia (Co-
575 PIs). The reinforcement layout of the wall was designed by the Co-PIs Prof. Carlos Blandon
576 and Prof. Ricardo Bonett. The test units TW2 and TW3 were financed through a grant by the
577 *Stiftung zur Förderung der Denkmalpflege* (“Trust for Cultural Heritage”), which also
578 supported the first author. The second author was supported by a grant of the *University of*

579 Cluj-Napoca, Romania, as well as a fellowship of the EPFL, while the third author was
580 supported by the SNSF grant 200021_132315 “Seismic design and assessment of reinforced
581 concrete core walls - Phase II”. All contributions are gratefully acknowledged. The authors
582 would also like to express their sincere appreciation to all engineers, technicians and students
583 who helped with the laboratory testing.

584

REFERENCES

585 Almeida, J. P., Prodan, O., Rosso, A., and Beyer, K., 2016. Tests on Thin Reinforced Concrete
586 Walls Subjected to In-Plane and Out-of-Plane Cyclic Loading. figshare.
587 <http://doi.org/10.6084/m9.figshare.3490754.v2>.

588 Almeida, J. P., Prodan, O., Tarquini, D., and Beyer, K., 2016. Influence of Lap Splices on the Cyclic
589 Inelastic Response of RC Walls. I: Database Assembly, New Experimental Tests, and Findings for
590 Model Development, *Journal of Structural Engineering* :(Manuscript under review).

591 Beyer, K., Dazio, A., and Priestley, M. J. N., 2008. Quasi-Static Cyclic Tests of Two U-Shaped
592 Reinforced Concrete Walls, *Journal of Earthquake Engineering* **12**, 1023–53.

593 Bimschas, M., 2010. *Displacement Based Seismic Assessment of Existing Bridges in Regions of*
594 *Moderate Seismicity, PhD Thesis*, ETH, Zurich, Switzerland.

595 Birely, A. C., 2012. *Seismic Performance of Slender Reinforced Concrete Structural Walls, PhD*
596 *Thesis*, University of Washington, Washington, U.S.

597 Brueggen, B. L., 2009. *Performance of T-Shaped Reinforced Concrete Structural Walls under*
598 *Multi-Directional Loading, PhD Thesis*, University of Minnesota, Twin Cities, USA.

599 Constantin, R., and Beyer, K., 2016. Behaviour of U-Shaped RC Walls under Quasi-Static Cyclic
600 Diagonal Loading, *Engineering Structures* **106**, 36–52.

601 Elnady, M. E., 2008. *Seismic Rehabilitation of RC Structural Walls, PhD Thesis*, McMaster
602 University, Hamilton, Canada.

603 Elwood, K. J., 2013. Performance of Concrete Buildings in the 22 February 2011 Christchurch
604 Earthquake and Implications for Canadian Codes, *Canadian Journal of Civil Engineering* **40**, 759–76.

605 Goodsir, W. J., 1985. *The Design of Coupled Frame-Wall Structures for Seismic Actions, PhD*
606 *Thesis*, University of Canterbury, Christchurch, New Zealand.

607 Hannewald, P., Bimschas, M., and Dazio, A., 2013. *Quasi-Static Cyclic Tests on RC Bridge Piers*
608 *with Detailing Deficiencies, Report Nr. 352 - Institut fur Baustatik und Konstruktion*, ETH, Zurich,
609 Switzerland.

610 HBM. 2000. Catman Data Acquisition Software. Hottinger Baldwin Messtechnik GmbH,

611 Darmstadt, Deutschland: <http://www.hbm.com/en/menu/products/software/data-acquisition-software>.

612 Johnson, B., 2010. *Anchorage Detailing Effects on Lateral Deformation Components of RC Shear*
613 *Walls, MSc Thesis*, University of Minnesota, Minneapolis, U.S.

614 Kam, W. Y., Pampanin, S., and Elwood, K., 2011. Seismic Performance of Reinforced Concrete
615 Buildings in the 22 February Christchurch (Lyttleton) Earthquake, *Bulletin of the New Zealand National*
616 *Society for Earthquake Engineering* **44**, 239–78.

617 Layssi, H., and Mitchell, D., 2012. Experiments on Seismic Retrofit and Repair of Reinforced
618 Concrete Shear Walls, in *Proceedings of the 6th International Conference on FRP Composites in Civil*
619 *Engineering (CICE)*, Rome, Italy.

620 NDI, 2009. Optotrak Certus HD, Northern Digital Inc. Waterloo, Ontario, Canada:
621 <http://www.ndigital.com/industrial/certushd.php>.

622 Oesterle, R. G., Fiorato, A. E., Johal, L. S., Carpenter, J. E., Russell, H. G., and Corley, W. G.,
623 1976. *Earthquake Resistant Structural Walls - Tests of Isolated Walls, Report to National Science*
624 *Foundation - Portland Cement Association*, Skokie, Illinois, U.S.

625 Paterson, J., and Mitchell, D., 2003. Seismic Retrofit of Shear Walls with Headed Bars and Carbon
626 Fiber Wrap, *Journal of Structural Engineering* **129**, 606–14.

627 Reynouard, J. M., and Fardis, M. N., 1993. *Shear Wall Structures, ECOEST/ICONS Thematic*
628 *report. No 5 - LNEC-National Laboratory of Civil Engineering*, Lisbon, Portugal.

629 Rosso, A., Almeida, J. P., and Beyer, K., 2016. Stability of Thin Reinforced Concrete Walls under
630 Cyclic Loads: State-of-the-Art and New Experimental Findings, *Bulletin of Earthquake Engineering*
631 **14**, 455–84.

632 Sritharan, S., Beyer, K., Henry, R. S., Chai, Y. H., Kowalsky, M. and Bull, D., 2014. Understanding
633 Poor Seismic Performance of Concrete Walls and Design Implications, *Earthquake Spectra* **30**, 307–
634 34.

635 Thomsen, J. H., and Wallace, J. W., 1995. *Displacement Based Design of Reinforced Concrete*
636 *Structural Walls: An Experimental Investigation of Walls with Rectangular and T-Shaped Cross-*
637 *Sections, Report No. CU/CEE-95-06 - Departement of Civil and Environmental Engineering*, Clarkson
638 University, Postdam, U.S.

639 Villalobos, E. J., 2014. *Seismic Response of Structural Walls with Geometric Reinforcement*
640 *Discontinuities, PhD Thesis*, Purdue University, Indiana, U.S.

641 Wallace, J. W., Massone, L. M., Bonelli, P., Dragovich, J., Lagos, R., Lüders, C., and Moehle, J.,
642 2012. Damage and Implications for Seismic Design of RC Structural Wall Buildings. *Earthquake*
643 *Spectra* **28**, S281–99.